


Heisenberg-Limited Quantum Metrology Using Collective Dephasing

Shingo Kukita^{1,*}, Yuichiro Matsuzaki^{2,†} and Yasushi Kondo^{1,‡}

¹*Department of Physics, Kindai University, Higashi-Osaka 577-8502, Japan*

²*Device Technology Research Institute, National Institute of Advanced Industrial Science and Technology (AIST), 1-1-1, Umezono, Tsukuba, Ibaraki 305-8568, Japan*

 (Received 22 March 2021; revised 16 June 2021; accepted 11 November 2021; published 10 December 2021)

The goal of quantum metrology is the precise estimation of parameters using quantum properties such as entanglement. This estimation usually consists of three steps: state preparation, time evolution during which information of the parameters is encoded in the state, and readout of the state. Decoherence during the time evolution typically degrades the performance of quantum metrology and is considered to be one of the major obstacles to realizing entanglement-enhanced sensing. We show, however, that under suitable conditions, this decoherence can be exploited to improve the sensitivity. Assume that we have two axes, and our aim is to estimate the relative angle between them. Our results reveal that the use of Markovian collective dephasing to estimate the relative angle between the two directions affords Heisenberg-limited sensitivity. Moreover, our protocol based on Markovian collective dephasing is robust against environmental noise: it is possible to achieve the Heisenberg limit by applying the collective dephasing even under the effect of independent dephasing. Our counterintuitive proposal with the decoherence leads to alternative applications in quantum metrology.

DOI: [10.1103/PhysRevApplied.16.064026](https://doi.org/10.1103/PhysRevApplied.16.064026)

I. INTRODUCTION

Sensing technology is useful for many practical applications [1–3], and an improved sensitivity is essential for practical purposes. Quantum metrology is a promising approach in order to improve the sensitivity using qubits owing to recent developments in quantum technology [4–14]. Quantum states can acquire a phase during interaction with the target fields. The readout of the phase provides information on the amplitude of the target fields [15–21]. Quantum sensing allows us to measure not only the amplitude of the fields but also many other quantities. Parameters that can be measured using qubit-based sensing include the Fourier coefficients of the spatially distributed fields [22], field gradient [23], frequency of ac magnetic fields [24], and rotation [25,26]. When n separable qubits are used as probes, the uncertainty of parameter estimation scales as $\mathcal{O}(1/\sqrt{n})$, which is called the standard quantum limit (SQL). By contrast, the uncertainty scales as $\mathcal{O}(1/n)$ when highly entangled states of qubits, such as Greenberger-Horne-Zeilinger (GHZ) states, are used [27–29]. This scaling is called the Heisenberg limit (HL) [9,18,30]. Many studies have been conducted to achieve Heisenberg-limited sensitivity [31–40].

In realistic situations, entangled qubits are affected by environmental noise during the time evolution required to encode the parameter information, and this decoherence is one of the main obstacles to realizing entanglement-enhanced sensors. If the noise acts independently on the qubits, the entanglement of the qubits rapidly disappears, and the states of the n qubits become separable. Thus, it is not trivial whether entanglement is useful. Numerous attempts have been made to address the problem of decoherence in order to overcome the SQL with entangled sensors [20,41–48]. Measurements in a quantum Zeno regime can be adopted to achieve a scaling of $\mathcal{O}(n^{3/4})$ if the noise is time-inhomogeneous independent dephasing [19,21,42,43,48–50]. In addition, quantum error correction can be applied to noisy metrology to suppress the effect of decoherence [51–55], and this method has been demonstrated by several experiments [56,57]. Quantum teleportation is another tool that protects quantum states from the effects of noise [48,58,59]. There is a protocol for reaching the HL in the estimation of the decay rate using dephasing [60,61]. Measurements of the environment itself improve the sensitivity of parameter estimation even under the effect of noise [62]. There are several other methods for improving the sensitivity of estimation under noise [22,63–66].

In this paper, we show that the decoherence can be useful to realize a robust quantum metrology protocol. More specifically, we consider estimation of the relative angle

*toranojoh@phys.kindai.ac.jp

†matsuzaki.yuichiro@aist.go.jp

‡ykondo@kindai.ac.jp

between two arbitrary axes by using collective dephasing. Two arbitrary axes here are, for example, determined by different quantization axes of electron spins at different spatial locations. In this case, the estimation of the relative angle is utilized to align the quantization axes. By using our approach, we can achieve the HL sensitivity in ideal conditions. Moreover, our calculations establish that our protocol using the collective dephasing is highly robust against noise; this protocol actually achieves the HL sensitivity even under the effect of independent noise from the environment.

In addition, the estimation of the relative angles between different axes is relevant in quantum-sensor networks. Quantum-sensing network is an emerging technology that has many potential applications such as detecting nonlocal quantities or sensing with security inbuilt [67–73]. We can use solid-state qubits such as electron spins for the quantum sensing. For the practical use of quantum-sensing network, the quantization axes of distant qubits should be aligned with the direction that we choose. As discussed above, our protocol to estimate the relative angle of two axes can be used for such a calibration of the quantum sensors.

This paper is organized as follows. Section II introduces the model with which a relative angle between two axes is measured with collective dephasing, while we analytically calculate its dynamics in Sec. III. We discuss the scaling behavior of our protocol in Secs. IV and V. We find that our protocol leads the HL. In Sec. V, we analyze the asymptotic behavior when the number of qubits are large. We discuss the case when collective noise for measurement is time inhomogeneous [74] in Sec. VI. Section VII is devoted to discussion of physical applications of our scheme. Section VIII concludes our work.

II. MODEL

Let us explain the setup of our estimation protocol. Suppose that Alice has an axis and Bob has another. Alice does not know the direction of Bob's axis and tries to estimate the relative angle between his axis and her own. The prescription of our protocol is as follows (Fig. 1). (i) Alice prepares qubits in a GHZ state according to her axis and sends the qubits to Bob. (ii) Bob applies global magnetic fields or the collective dephasing noise along his axis on the qubits he received and sends them back to Alice. (iii) Alice reads out the state. (iv) They repeat these three steps M times. We have $M = T/(t_{\text{prep}} + t + t_{\text{read}})$, where T denotes the total time allowed for the protocol, t_{prep} denotes the time needed to prepare the GHZ state (which includes the transportation time), t denotes the evolution time, and t_{read} denotes the time required to read out the state. Throughout this paper, we assume that the GHZ state can be prepared and read out in a much shorter time scale than the evolution time, and we obtain $M \simeq T/t$.

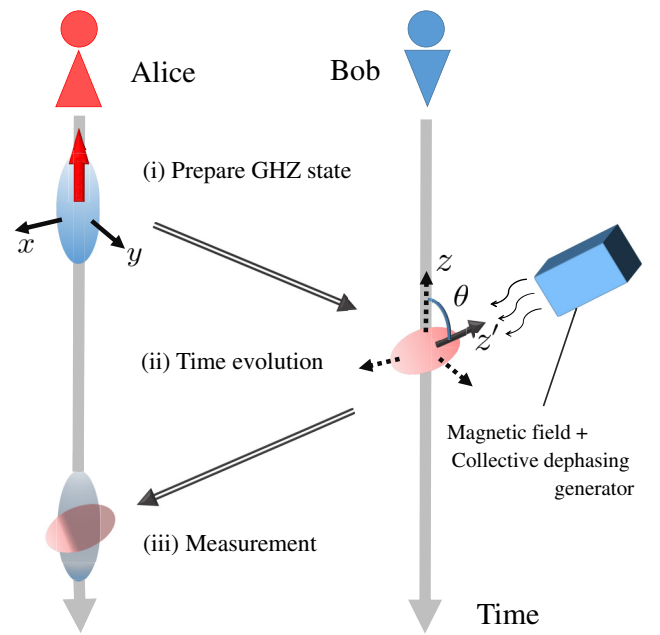


FIG. 1. Schematic illustration of the proposed protocol. (i) Alice prepares a GHZ state, (ii) Bob receives this state and lets it evolve under the applied collective noise (or a global magnetic field), and (iii) Alice measures this state.

Let us explain the details of our setup. We define Alice's (Bob's) axis as the z (z') axis. In step (i), Alice prepares n qubits in a GHZ state, which is defined as follows:

$$|\phi_{\text{GHZ}}\rangle = \frac{1}{\sqrt{2}}(|\uparrow\uparrow\cdots\uparrow\rangle_z + |\downarrow\downarrow\cdots\downarrow\rangle_z), \quad (1)$$

where $|\uparrow\rangle_z$ ($|\downarrow\rangle_z$) is the eigenstate of σ_z with an eigenvalue of $+1$ (-1), and $|\uparrow\uparrow\cdots\uparrow\rangle_z$ denotes $|\uparrow\rangle_z \otimes |\uparrow\rangle_z \otimes \cdots \otimes |\uparrow\rangle_z$. Here we take the ordinary notation of the Pauli matrices as follows:

$$\sigma_x = \begin{pmatrix} 0 & 1 \\ 1 & 0 \end{pmatrix}, \quad \sigma_y = \begin{pmatrix} 0 & -i \\ i & 0 \end{pmatrix}, \quad \sigma_z = \begin{pmatrix} 1 & 0 \\ 0 & -1 \end{pmatrix}. \quad (2)$$

Note that the x and y axes are actually fixed when the relative phase in the GHZ state is fixed.

In step (ii), to encode the information on the relative angle, Bob applies the collective dephasing noise or a global magnetic field (a rival protocol) along the z' axis to the GHZ state that he receives from Alice. In addition, we assume that environmental Markovian dephasing noise independently affects each qubit along the z' axis. We introduce the vector

$$\vec{z}' = (\sin\theta \cos\phi, \sin\theta \sin\phi, \cos\theta), \quad (3)$$

which is the unit vector along the z' direction represented in the (x, y, z) coordinates of Alice. θ is the parameter to be

estimated. The Pauli matrix along the z' direction is written as

$$\sigma_{z'} = \vec{z}' \cdot \vec{\sigma} = \begin{pmatrix} \cos \theta & e^{-i\phi} \sin \theta \\ e^{i\phi} \sin \theta & -\cos \theta \end{pmatrix}. \quad (4)$$

Accordingly, the eigenstates of $\sigma_{z'}$ are defined as

$$\begin{aligned} |\uparrow\rangle_{z'} &= \frac{1}{\sqrt{2}} \left(\sqrt{1 + \cos \theta} |\uparrow\rangle_z + e^{i\phi} \sqrt{1 - \cos \theta} |\downarrow\rangle_z \right), \\ |\downarrow\rangle_{z'} &= \frac{1}{\sqrt{2}} \left(-\sqrt{1 - \cos \theta} |\uparrow\rangle_z + e^{i\phi} \sqrt{1 + \cos \theta} |\downarrow\rangle_z \right), \end{aligned} \quad (5)$$

whose eigenvalues are 1 and -1 , respectively.

In addition, we use the notation $\sigma_\alpha^{(l)}$ ($\alpha = x, y, z, x', y', z'$) for a Pauli matrix acting only on the l th qubit, e.g., $\sigma_\alpha^{(1)} = \sigma_\alpha \otimes \mathbb{I} \cdots \otimes \mathbb{I}$, where \mathbb{I} is the 2×2 identity matrix. Thus, the dynamics of the GHZ state on Bob's side is described as follows:

$$\begin{aligned} \frac{d\rho}{dt} &= -i[\Omega L_{z'}, \rho] + \gamma_C \left(L_{z'} \rho L_{z'} - \frac{1}{2} \{L_{z'}^2, \rho\} \right) \\ &+ \gamma_I \sum_{l=1}^n (\sigma_{z'}^{(l)} \rho \sigma_{z'}^{(l)} - \rho), \end{aligned} \quad (6)$$

where $L_\alpha = \sum_{l=1}^n \sigma_\alpha^{(l)}$. $\Omega, \gamma_C, \gamma_I$ characterize the strength of the global magnetic field, collective dephasing, and independent dephasing, respectively. Throughout this paper, we take $\hbar = 1$. Alice and Bob can tune γ_C and Ω , whereas γ_I is uncontrollable. We also take $\phi = 0$ for simplicity. We show that our protocol for estimating θ does not depend on the value of ϕ in the parameter regime of interest in Sec. III. The goal is to estimate the azimuthal angle θ with high precision by measuring the state ρ after the above dynamics.

III. DYNAMICS DURING ENCODING PROCESS

The exact solution of Eq. (6) is analytically given. The reader who may be interested in the detailed analytical calculation should also refer to Appendix A.

Here, let us consider the case of $\gamma_I = 0$. To this end, it is convenient to introduce the following Young-Yamanouchi basis, according to group representation theory [75–78], which is characterized as follows:

$$\begin{aligned} |j, m, i\rangle_z &\in \mathbb{C}^{2^n}, \\ j_{\min} &\leq j \leq n/2, \\ -j &\leq m \leq j, \\ 1 &\leq i \leq d_n^j = \frac{(2j+1)n!}{(n/2+j+1)!(n/2-j)!}, \end{aligned}$$

$$\begin{aligned} \frac{L_z}{2} |j, m, i\rangle_z &= m |j, m, i\rangle_z, \\ L_+ |j, m, i\rangle_z &:= \frac{L_x + iL_y}{2} |j, m, i\rangle_z \\ &= \sqrt{j(j+1) - m(m+1)} |j, m+1, i\rangle_z, \\ L_- |j, m, i\rangle_z &:= \frac{L_x - iL_y}{2} |j, m, i\rangle_z \\ &= \sqrt{j(j+1) - m(m-1)} |j, m-1, i\rangle_z, \\ \frac{1}{4} L^2 |j, m, i\rangle_z &:= \frac{1}{4} (L_x^2 + L_y^2 + L_z^2) |j, m, i\rangle_z \\ &= j(j+1) |j, m, i\rangle_z, \end{aligned} \quad (7)$$

where j_{\min} is 0 (1/2), and j, m take integers (half-integers) for even (odd) n . The index i represents the number of ways of composing n spins to obtain the total angular momentum j . We refer to this basis as the irrep. basis hereinafter. The following calculations might seem to be difficult at the first look. However, the calculations are done only by substituting the properties Eq. (7).

Note that the same relations are valid for Bob's axes when x, y, z are replaced by x', y', z' , respectively. We introduce the x' and y' axes, which are orthogonal to Bob's z' axis. The choice of these axes has rotational ambiguity and Bob can take any pair of these axes as the x' and y' axes. However, we do not discuss the explicit direction of the x' and y' axes because this does not affect the estimation of θ . Note, also, that the operator L^2 is invariant under the coordinate transformation and thus $L^2 = L_{x'}^2 + L_{y'}^2 + L_{z'}^2$ is satisfied.

For $j = n/2$, we simply represent the irrep. basis $|n/2, m, 1\rangle_{z(z')}$ ($d_n^j = 1$ in this case) in terms of $|\uparrow(\downarrow)\rangle_{z(z')}$ as

$$\begin{aligned} |n/2, m, 1\rangle_{z(z')} &= \frac{1}{\sqrt{n C_{m+n/2}}} \left(\underbrace{|\uparrow \uparrow \cdots \uparrow}_{m+n/2} \underbrace{|\downarrow \cdots \downarrow}_{n/2-m} \right)_{z(z')} \\ &+ (\text{all the other permuted states}). \end{aligned} \quad (8)$$

In terms of the irrep. basis, $|\phi_{\text{GHZ}}\rangle$ is described as

$$\begin{aligned} |\phi_{\text{GHZ}}\rangle &= (|\uparrow \uparrow \cdots \uparrow\rangle_z + |\downarrow \downarrow \cdots \downarrow\rangle_z) / \sqrt{2} \\ &= (|n/2, n/2, 1\rangle_z + |n/2, -n/2, 1\rangle_z) / \sqrt{2}. \end{aligned} \quad (9)$$

We emphasize that we can expand this vector in terms of $|\uparrow(\downarrow)\rangle_z$ as follows:

$$|n/2, m, 1\rangle_{z'} = \sum_{-n/2 \leq m' \leq n/2} C_{mm'} |n/2, m', 1\rangle_z, \quad (10)$$

where the summation in the rhs runs only over m' . This is because $L^2 = L_x^2 + L_y^2 + L_z^2 = L_{x'}^2 + L_{y'}^2 + L_{z'}^2$. This

expression is also understood in terms of permutation symmetry. Let U denote the unitary matrix whose action is $U|\uparrow(\downarrow)\rangle_z = |\uparrow(\downarrow)\rangle_{z'}$. The unitary U changes the coordinate index z to z' . According to Eq. (8), the transformation between the irrep. basis in both the z and z' representations is given as

$$\begin{aligned} |n/2, m, 1\rangle_{z'} &= U^{(1)} \dots U^{(l)} \dots U^{(n)} |n/2, m, 1\rangle_z \\ &= \left(\prod_{l=1}^n U^{(l)} \right) |n/2, m, 1\rangle_z, \end{aligned} \quad (11)$$

where the index l indicates that $U^{(l)}$ acts only on the l th qubit. Because $\prod_{l=1}^n U^{(l)}$ is invariant under any permutation of the qubits, $|n/2, m, 1\rangle_{z'}$ is symmetric under permutation even in terms of $|\uparrow(\downarrow)\rangle_z$ (as $|n/2, m, 1\rangle_z$ is symmetric). Thus, $|n/2, m, 1\rangle_{z'}$ is represented as the sum of $\{|n/2, m, 1\rangle_z\}_{m \leq n/2}$, as shown in Eq. (10).

For later convenience, we define the matrix elements

$$\overline{|j, m\rangle_{z'} \langle j, m'|} := \frac{1}{d_n^j} \sum_{i=1}^{d_n^j} |j, m, i\rangle_{z'} \langle j, m', i|, \quad (12)$$

because the operations we address below are independent of the index i . A relevant point is that the dynamics of $\overline{|j, m\rangle_{z'} \langle j, m'|}$ caused by the right-hand side of the Lindblad equation (6) with $\gamma' = 0$ is easily calculated by using

Eqs. (7).

$$\begin{aligned} &-i[\Omega L_{z'}, \overline{|j, m\rangle_{z'} \langle j, m'|}] \\ &+ \gamma_C \left(L_{z'} \overline{|j, m\rangle_{z'} \langle j, m'|} L_{z'} - \frac{1}{2} \{L_{z'}^2, \overline{|j, m\rangle_{z'} \langle j, m'|}\} \right) \\ &= (-2i\Omega(m - m') - 2\gamma_C(m - m')^2) \overline{|j, m\rangle_{z'} \langle j, m'|}. \end{aligned} \quad (13)$$

Also, we find that the initial state $\rho(0) = |\phi_{\text{GHZ}}\rangle\langle\phi_{\text{GHZ}}|$ can be rewritten using Eq. (10):

$$\rho(0) = \sum_{-n/2 \leq m, m' \leq n/2} \rho_{m, m'} \overline{|n/2, m\rangle_{z'} \langle n/2, m'|}, \quad (14)$$

where $\rho_{m, m'} = {}_{z'}\langle n/2, m, 1 | \phi_{\text{GHZ}} \rangle \langle \phi_{\text{GHZ}} | n/2, m', 1 \rangle_{z'}$. We note that $d_n^{n/2} = 1$, or equivalently, $\overline{|n/2, m\rangle_{z'} \langle n/2, m'|} = |n/2, m, 1\rangle_{z'} \langle n/2, m', 1|$.

Then $\rho(t)$ when $\gamma_I = 0$ is given as

$$\begin{aligned} \rho_{\gamma_I=0}(t) &= \sum_{-n/2 \leq m, m' \leq n/2} e^{-2i\Omega(m-m')t - 2\gamma_C(m-m')^2 t} \rho_{m, m'} \\ &\times \overline{|n/2, m\rangle_{z'} \langle n/2, m'|}. \end{aligned} \quad (15)$$

Note that the explicit form of $\rho_{m, m'}$ is given as

$$\begin{aligned} \rho_{m, m'} &= \frac{\sqrt{{}_n C_{(n/2)+m} {}_n C_{(n/2)+m'}}}{2^{n+1}} \left((\sqrt{1 + \cos \theta})^{(n/2)+m} (-\sqrt{1 - \cos \theta})^{(n/2)-m} \right. \\ &+ e^{-i\phi} (\sqrt{1 - \cos \theta})^{(n/2)+m} (\sqrt{1 + \cos \theta})^{(n/2)-m} \left. \right) \left((\sqrt{1 + \cos \theta})^{(n/2)+m'} (-\sqrt{1 - \cos \theta})^{(n/2)-m'} \right. \\ &+ e^{i\phi} (\sqrt{1 - \cos \theta})^{(n/2)+m'} (\sqrt{1 + \cos \theta})^{(n/2)-m'} \left. \right). \end{aligned} \quad (16)$$

The key insight is that we have a rapid decay of the nondiagonal terms with a rate of $\gamma_C(m - m')^2$. This means that, if we have $|m - m'| = \mathcal{O}(n)$, the decay rate is an order of $\mathcal{O}(n^2)$. This is the notable feature of the collective behavior of the entanglement, and such a rapid decay is the key to achieve the HL in our scheme as we explain later.

We also calculate the dynamics of the density matrix with $\gamma_I \neq 0$ in Appendix A, which is rather technical. It is worth mentioning that the index i is set to be $i = 1$ throughout the calculations above because $j = n/2$ is satisfied in whole dynamics. However, this is valid only for the case of $\gamma_I = 0$. When we consider the case of $\gamma_I \neq 0$, we have to take into account the contribution of all i 's and j 's, and this is the reason why the calculations are rather complicated.

IV. SENSITIVITY SCALING WITH MARKOVIAN COLLECTIVE DEPHASING

We show the advantages of our protocol in which Bob uses collective dephasing for encoding the information of the z' axis on a GHZ state (hereafter, called protocol D, after dephasing) over that using the global magnetic field (hereafter, called protocol F, after global magnetic field) in terms of the robustness against independent dephasing by observing the sensitivity scaling.

To quantify the sensitivity, we can use either the classical Fisher information or quantum Fisher information. Once we fix a positive operator-valued measure (POVM) $\{\Pi_I\}$ to measure the final state, the uncertainty

of the estimation is bounded by the following Cramér-Rao bound:

$$\delta\theta \geq \delta\theta^{\min} := 1/\sqrt{MF_{\theta}(\{\Pi_I\})}, \quad (17)$$

where $M = T/t$ is the trial number and $F_{\theta}(\{\Pi_I\})$ is the Fisher information. See Appendix B for the details of the Fisher information and the Cramér-Rao bound. Throughout our paper, we discuss the performance of the estimation scheme by focusing only on $\delta\theta^{\min}$ and do not care about $\delta\theta$ itself.

In quantum estimation, we can further minimize the uncertainty $\delta\theta^{\min}$ by choosing the best POVMs. We have the following quantum Cramér-Rao bound for any POVM $\{\Pi_I\}$:

$$\delta\theta^{\min} \geq \delta\theta^{(Q)\min} := 1/\sqrt{MF_{\theta}^{(Q)}}, \quad (18)$$

where $F_{\theta}^{(Q)}$ is the quantum Fisher information defined in Appendix B.

For protocol D, we find an appropriate POVM, with which we can attain the HL scaling, as shown later, and we use $\delta\theta^{\min}$ to quantify the uncertainty. Meanwhile, for protocol F, we adopt $\delta\theta^{(Q)\min}$. Either uncertainty of $\delta\theta^{\min}$ or $\delta\theta^{(Q)\min}$ depends on the evolution time t . Hence, we need to optimize t for the uncertainty to take the smallest value.

We find that a projective measurement defined by the operator $\mathcal{P} = |\phi_{\text{GHZ}}\rangle\langle\phi_{\text{GHZ}}|$ is an appropriate measurement in protocol D. This projection provides a survival probability $P(t) := \langle\phi_{\text{GHZ}}|\rho(t)|\phi_{\text{GHZ}}\rangle$ in step (iii). Then, Alice estimates the value of θ by analyzing the M outcomes. The uncertainty of this estimation scheme is determined by

$$\delta\theta^{\min} = \frac{\sqrt{P(t)[1-P(t)]}}{|dP(t)/d\theta|\sqrt{M}} = \frac{\sqrt{P(t)[1-P(t)]}}{|dP(t)/d\theta|\sqrt{T/t}}. \quad (19)$$

We find that $|\phi_{\text{GHZ}}\rangle\langle\phi_{\text{GHZ}}|$ leads to the uncertainty achieving the HL scaling, as shown in Fig. 2. Therefore, $\delta\theta^{\min}$ is employed for the case of protocol D.

It is worth mentioning that we calculate the ultimate bound of the sensitivity using an optimal POVM for protocol F while we calculate the sensitivity using a specific projective measurement for protocol D. The reason for this is to show a practical advantage of protocol D over protocol F. For protocol F, the form of the optimal POVM is unknown for us. On the other hand, we know the explicit form of the measurement for protocol D. This means that the sensitivity bound protocol D can be actually achieved while we do not know how to achieve the bound for protocol F. Note that \mathcal{P} is not necessarily the best measurement. If we could find the optimized measurement basis in protocol D, we could improve the sensitivity by a constant factor.

Figure 2(a) shows the scaling behavior of the minimized uncertainty $\delta\theta^{\min}$ in protocol D ($\delta\theta^{(Q)\min}$ in protocol F)

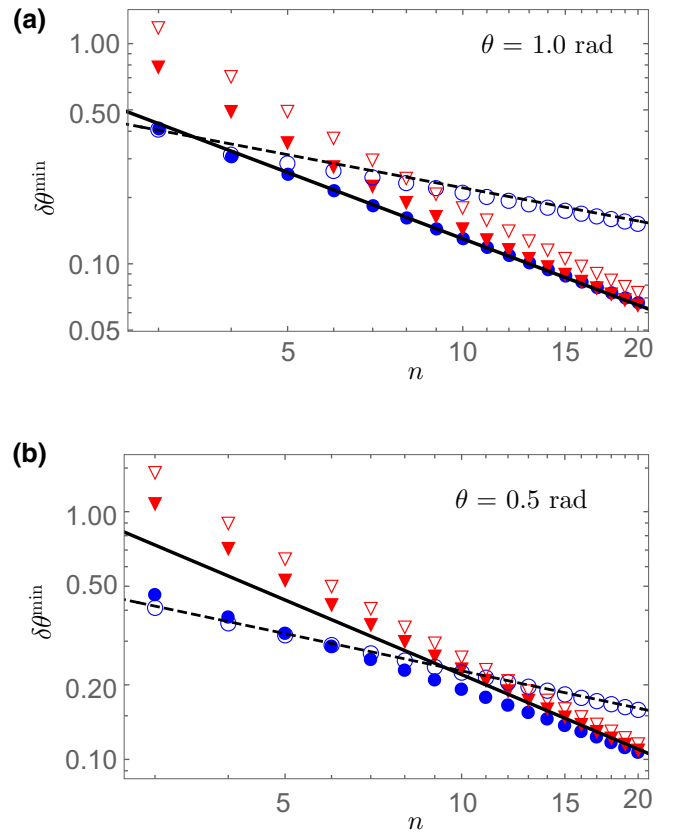


FIG. 2. $\delta\theta^{\min}$ in protocol D ($\delta\theta^{(Q)\min}$ in protocol F) versus the number of qubits n for (a) $\theta = 1.0$ rad and (b) $\theta = 0.5$ rad. In both panels, the filled (open) triangles represent $\delta\theta^{\min}$ with the parameters $\Omega = 0$, $\gamma_C = 1$, and $\gamma_I = 0(1)$, whereas the filled (open) circles represent $\delta\theta^{(Q)\min}$ with the parameters $\Omega = 1$, $\gamma_I = 0$, and $\gamma_C = 0(1)$. The solid (dashed) line shows the HL (SQL). The total time T is taken as $T = 1$.

versus the number of qubits n for $(\Omega, \gamma_C, \gamma_I) = (0, 1, 0)$ and $(0, 1, 1)$ [(1, 0, 0) and (1, 0, 1)] when $\theta = 1.0$ rad, while Fig. 2(b) does the case when $\theta = 0.5$ rad. In the noiseless cases of $(\Omega, \gamma_C, \gamma_I) = (1, 0, 0)$ and $(0, 1, 0)$ in Fig. 2, both $\delta\theta^{\min}$ in protocol D and $\delta\theta^{(Q)\min}$ in protocol F approach the HL for large n . However, protocol F is fragile against independent dephasing [$(\Omega, \gamma_C, \gamma_I) = (1, 0, 1)$] in the sense that $\delta\theta^{(Q)\min}$ scales as the SQL. By contrast, protocol D is robust against independent dephasing [$(\Omega, \gamma_C, \gamma_I) = (0, 1, 1)$]: $\delta\theta^{\min}$ scales as the HL. Therefore, protocol D outperforms protocol F for large n . Note that a specific measurement basis ($|\phi_{\text{GHZ}}\rangle\langle\phi_{\text{GHZ}}|$) is chosen in protocol D while the uncertainty in protocol F is evaluated on the basis of the quantum Fisher information without knowledge of the explicit form of the POVM to employ.

V. ASYMPTOTIC BEHAVIOR OF SCALING

To understand the origin of the robustness of protocol D, we analytically evaluate the scaling behavior of the

minimized uncertainty $\delta\theta^{\min}$ under the effect of independent dephasing for large n . In the short-time region, $P(t)$ is approximately given as (see Appendix C),

$$P(t) \sim 1 - \gamma_C t [n^2 \cos^2 \theta + n(1 - \cos^2 \theta)] - \gamma_I t n. \quad (20)$$

If we consider protocol D with an assigned evolution time of $t = t_0/n^2$ where t_0 denotes a time constant, we find that $P(t)$ and $1 - P(t)$ scale as $\mathcal{O}(n^0)$. In addition, $|dP(t)/dt|$ also has the $\mathcal{O}(n^0)$ dependence. This result implies that the minimized uncertainty, Eq. (19), scales as

$$\delta\theta^{\min} = \frac{\mathcal{O}(n^0)}{\mathcal{O}(n^0)\sqrt{n^2 T/t_0}} = \mathcal{O}(n^{-1}), \quad (21)$$

for large n , which is the HL scaling. Thus, by utilizing the short-time perturbation, we show that protocol D achieves the HL even under the influence of independent dephasing. The reason why protocol D is robust against independent noise is that the dynamics due to the collective dephasing is faster than that of the independent dephasing: we can find the time scale where only collective dephasing is significant. Note that θ can be estimated without knowing the value of ϕ in a short-time regime because $P(t)$ is independent of ϕ in this regime.

We provide a possible reason of why our protocol achieves the HL even under the effect of independent decoherence. When we use a global magnetic field, the information of the relative angle is encoded into the phase of the state. The independent decoherence destroys the phase information. Meanwhile, our protocol to use the collective dephasing encodes the information of the relative angle into the decaying behavior of the state. Since the contribution of independent dephasing to the state is similar to that of the collective dephasing, the influence of the independent noise is insignificant. Therefore, the effect of the independent decoherence is not significant in our protocol D.

In our protocol, we focus only on independent dephasing. However, the above calculation also works for any type of independent noise. According to the definition of the independence of noise, any independent noise behaves as approximately $\gamma_I t n$ in a short-time region, like the last term in Eq. (20). Thus, if the n^2 term in Eq. (20) is present (or equivalently, if collective dephasing noise exists), we achieve the HL under any independent noise in the same manner as in the above discussion.

VI. SENSITIVITY SCALING WITH TIME-INHOMOGENOUS COLLECTIVE DEPHASING

In quantum metrology, the sensitivity under Markovian noise could be very different from that under

the time-inhomogeneous one [20,42,43]. The time-inhomogeneous noise model takes into account the finite correlation time of the environment, whereas the Markovian environment has an infinitesimally short correlation time. Owing to the finite correlation time, a typical time-inhomogeneous noise model interpolates between exponential decay (which is typically observed in Markovian noise) and quadratic decay.

We investigate the sensitivity of our protocol when we use time-inhomogeneous collective dephasing for estimation in protocol D, hereafter called protocol D_{non} . In particular, we adopt a spin-boson model with a Lorentzian spectral density to consider the effect of the finite correlation time. This model was analyzed in Ref. [43], and the time-dependent decay rate was calculated as

$$\gamma_C(t) = \frac{\gamma_0 \tau_c}{t} (-1 + e^{-t/\tau_c} + t/\tau_c), \quad (22)$$

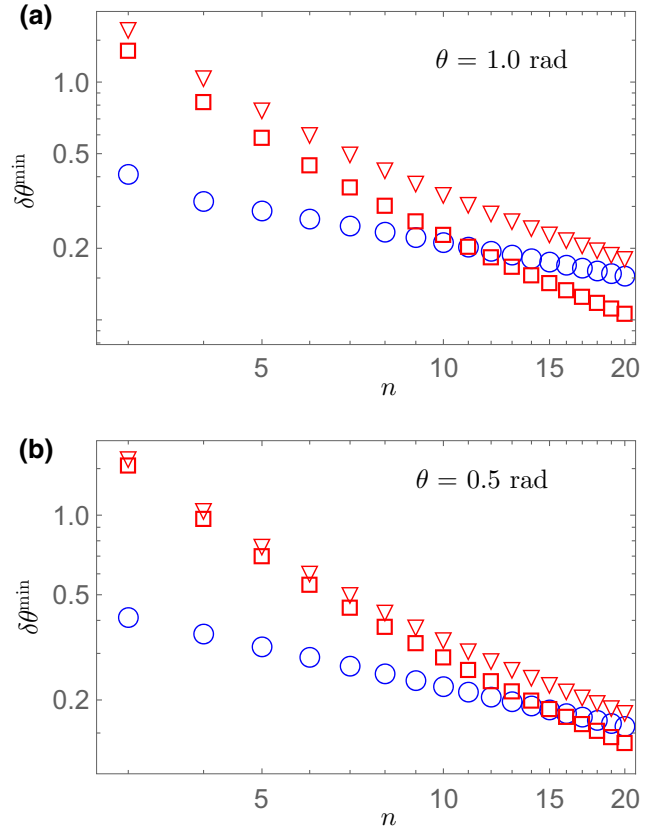


FIG. 3. Minimized uncertainty $\delta\theta^{\min}$ in protocol D_{non} ($\delta\theta^{(Q)\min}$ in protocol F) versus the number of qubits n for (a) $\theta = 1.0$ rad and (b) $\theta = 0.5$ rad. In both panels, the circles represent $\delta\theta^{(Q)\min}$ with parameters $\Omega = 1$, $\gamma_0 = 0$, and $\gamma_I = 1$, which give the same results as in Figs. 2(a) and 2(b). In (a), the triangles (squares) represent the uncertainty with parameters $\Omega = 0$, $\gamma_0 = 1$, $\tau_c = 0.01$ (0.001), and $\gamma_I = 1$, whereas the triangles (squares) in (b) show the uncertainty with parameters $\Omega = 0$, $\gamma_0 = 1$, $\tau_c = 0.005$ (0.0001), and $\gamma_I = 1$.

where τ_c denotes the correlation time. This decay rate interpolates between exponential decay and quadratic decay. For a short (long) correlation time, $\tau_c \ll t$ ($\tau_c \gg t$), we obtain $\gamma_C(t) \simeq \gamma_0$ [$\gamma_C(t) \simeq (\gamma_0 t / 2\tau_c)$]. Note that τ_c is a tunable parameter in this paper.

We compare $\delta\theta^{\min}$ in protocol D_{non} with $\delta\theta^{(\mathcal{Q})\min}$ in protocol F by performing numerical simulations. The results are shown in Figs. 3(a) and 3(b), where we take $\theta = 1.0$ and 0.5 rad, respectively. In the numerical simulations, we observe that either protocol D_{non} or protocol F approaches the SQL. Whether protocol D_{non} is advantageous over protocol F depends on both τ_c and θ . Figure 3 shows that protocol D_{non} outperforms protocol F when we take a sufficiently small τ_c . For $\theta = 1.0$ rad, $\tau_c = 0.001$ is sufficiently small, whereas $\tau_c \sim 0.0001$ is required for $\theta = 0.5$ rad. We emphasize that protocol D_{non} can outperform protocol F for any θ if we take sufficiently small τ_c , because the scaling behavior of $\delta\theta^{\min}$ achieves the HL in the Markovian limit $\tau_c \rightarrow 0$. We consider a threshold of the correlation time τ_{lim}^θ that characterizes whether $\delta\theta^{\min}$ in protocol D_{non} overcomes $\delta\theta^{(\mathcal{Q})\min}$ in protocol F, and discuss how we can approximately explain the θ dependence of τ_{lim}^θ in Appendix D.

VII. DISCUSSION

We discuss possible applications of our protocol. Our protocol to measure a relative angle between two axes is useful for quantum-sensor networks. When the quantity of interest is not local but has a global property, quantum-sensor networks can be used [67–70,72]. Entangled quantum sensors are spatially distributed, and they interact with target fields to extract the information about the parameters of interest. It is known that such quantum-sensing networks offer an advantage for some problems such as a NMR imaging [68], measuring field gradient [79], detecting a spatial Fourier coefficient [80], and sensing signals in an anonymous way [73]. To implement these protocols, it is usually assumed that the experimentalist knows a precise direction of a quantization axis of each quantum sensor. Moreover, it is desirable that the quantization axes of all sensors are aligned in the same direction, because otherwise a complicated calibration procedure is needed. Our protocol allows Alice to measure a relative angle between an axis of her qubits and that of Bob's qubits, and this is useful to make the quantization axes of the qubits aligned in the same direction, which is crucial for the application of quantum-sensing networks.

Also, our protocol could contribute to clock synchronization. We note that the synchronization of time in different systems has been interested in and practically relevant since Einstein's times [81]. Recently, clock synchronization based on quantum states was proposed [82,83]. However, one of the challenges of the quantum clock synchronization is to have a common phase

reference. Superposition states such as $|+\rangle = \frac{1}{\sqrt{2}}(|0\rangle + |1\rangle)$ are defined up to a local phase shift. If an x -axis direction of Alice is the same as that of Bob, they can prepare a state of $|+\rangle$, an eigenstate of σ_x without the common phase reference, because the axis direction plays the role of the common reference. Hence, our protocol has a potential to be utilized for such a clock synchronization. However, since our scheme requires the GHZ state to be sent from Alice to Bob, we need a stable quantum channel where the axis of the qubit is fixed during the transmission for the purpose explained above. To assess its suitability, further research may be needed, and we leave this as a future work.

Let us discuss the possible physical realization of our scheme. The main difficulty of our scheme is the transfer of quantum states from one place to another. However, in the Stern-Gerlach experiments [84], atoms can travel for macroscopic distances, while keeping the quantum nature of the spins. This clearly shows the potential to realize such a transfer of quantum states.

Another example of a traveling quantum object is a nuclear spin in a molecule solved in liquid. The nuclear spin can diffuse in liquid or flow with liquid while keeping its spin state. This property is employed for measuring a diffusion constant or a flow speed of the liquid [85]. Moreover, a quantum state of an electron spin can be transferred to that of a polarization of an optical photon [86–93], and so we could use the optical photons to send the quantum states. For the experimental demonstration, we must be concerned about decrease of the fidelity of the quantum states during the transfer. There will be several sources that cause the decoherence. For example, the spatially fluctuated external field coupling induces nuclear spins in liquid. Local temperature variations cause decoherence when we use optical photons to transfer the quantum states. To realize our scheme, it is necessary to overcome such difficulties, but a more detailed analysis is out of the scope of our paper.

We note that experimental realization of dephasing was reported in Refs. [94–96]. This shows a feasibility of our scheme to add collective dephasing.

VIII. CONCLUSION

In conclusion, we propose to use collective dephasing to improve the precision of quantum metrology. Assume that we have two axes, and our aim is to estimate the relative angle between them. Suppose that Alice has an axis, and Bob has another. Alice does not know Bob's one and tries to estimate the relative angle between his axis and hers. Alice generates a GHZ state according to her axis and sends it to Bob. Bob decoheres the received state by inducing collective Markovian dephasing along his own axis. This protocol achieves the HL for estimating the direction of Bob's axis under ideal conditions. Moreover, we show that the protocol using collective dephasing

is robust against noise; it achieves the HL even under the effect of independent Markovian dephasing on each qubit caused by the environment. This is in stark contrast to the conventional protocol that uses unitary dynamics for encoding the information, which cannot overcome the SQL under the effect of such noise. Although we discuss primarily the independent dephasing noise, our conclusion that the HL can be achieved is guaranteed even when the system is affected by arbitrary types of independent decoherence.

ACKNOWLEDGMENTS

This work is supported by the Leading Initiative for Excellent Young Researchers, MEXT, Japan; JST Presto (Grant No. JPMJPR1919) Japan; CREST (Grant No. JPMJCR1774); and JSPS KAKENHI (Grant No. 21K03423).

APPENDIX A: CALCULATION OF DYNAMICS FOR THE $\gamma_I \neq 0$ CASE

Here, we consider the case of $\gamma_I \neq 0$. Because the independent dephasing term in Eq. (6) commutes with the other two terms, it is sufficient to consider its action independently. The dynamical equation with only the third term at the right-hand side in Eq. (6) is easily solved and thus the exact solution for $\gamma_I \neq 0$ is written as follows:

$$\rho(t) = \mathcal{E}_t^{(n)} \cdots \mathcal{E}_t^{(l)} \cdots \mathcal{E}_t^{(1)} [\rho_{\gamma_I=0}(t)], \quad (A1)$$

$$\mathcal{E}_t^{(l)}(\rho) := \alpha(t)\rho + \beta(t)\sigma_{z'}^{(l)}\rho\sigma_{z'}^{(l)},$$

where $\alpha(t) := [(1 + e^{-2\gamma_I t})/2]$, and $\beta(t) := [(1 - e^{-2\gamma_I t})/2]$. We rearrange Eq. (A1) as

$$\begin{aligned} \mathcal{E}_t^{(n)} \cdots \mathcal{E}_t^{(l)} \cdots \mathcal{E}_t^{(1)} [\rho_{\gamma_I=0}(t)] &= \alpha^n(t)\rho_{\gamma_I=0}(t) + \alpha^{n-1}(t)\beta(t) \sum_l \sigma_{z'}^{(l)} \rho_{\gamma_I=0}(t) \sigma_{z'}^{(l)} + \alpha^{n-2}(t)\beta^2(t) \\ &\quad \times \sum_{1 \leq l_1 < l_2 \leq n} \sigma_{z'}^{(l_1)} \sigma_{z'}^{(l_2)} \rho_{\gamma_I=0}(t) \sigma_{z'}^{(l_1)} \sigma_{z'}^{(l_2)} + \cdots + \beta^n(t) \sigma_{z'}^{(1)} \sigma_{z'}^{(2)} \cdots \sigma_{z'}^{(n)} \rho_{\gamma_I=0}(t) \sigma_{z'}^{(1)} \sigma_{z'}^{(2)} \cdots \sigma_{z'}^{(n)} \\ &= \sum_{k=0}^n \left(\alpha^{n-k}(t) \beta^k(t) \sum_{1 \leq l_1 < l_2 < \cdots < l_k \leq n} \sigma_{z'}^{(l_1)} \sigma_{z'}^{(l_2)} \cdots \sigma_{z'}^{(l_k)} \rho_{\gamma_I=0}(t) \sigma_{z'}^{(l_1)} \sigma_{z'}^{(l_2)} \cdots \sigma_{z'}^{(l_k)} \right), \end{aligned} \quad (A2)$$

where we assign $\alpha^n(t)\rho_{\gamma_I=0}(t)$ as the $k=0$ term. For convenience of notation, we rewrite the above expression in terms of the irrep. basis. To this end, we introduce the coefficients $A_{j,m,m'}^{(k)}$ as follows:

$$\sum_j A_{j,m,m'}^{(k)} \overline{|j, m\rangle_{z'} \langle j, m'|} := \sum_{1 \leq l_1 < l_2 < \cdots < l_k \leq n} \sigma_{z'}^{(l_1)} \sigma_{z'}^{(l_2)} \cdots \sigma_{z'}^{(l_k)} \overline{|n/2, m\rangle_{z'} \langle n/2, m'|} \sigma_{z'}^{(l_1)} \sigma_{z'}^{(l_2)} \cdots \sigma_{z'}^{(l_k)}. \quad (A3)$$

By using Eqs. (A3) and (15), we obtain the exact solution of the dynamics with global magnetic field, collective noise and an independent one in a more convenient form:

$$\rho(t) = \sum_{k=0}^n \left(\alpha^{n-k}(t) \beta^k(t) \sum_{j=j_{\min}}^{n/2} \sum_{-j \leq m, m' \leq j'} e^{-2i\Omega(m-m')t - 2\gamma_C t(m-m')^2} \rho_{m,m'} A_{j,m,m'}^{(k)} \overline{|j, m\rangle_{z'} \langle j, m'|} \right). \quad (A4)$$

We show below that $A_{j,m,m'}^{(k)}$ are iteratively calculated by

$$\begin{aligned} A_{j,m,m'}^{(k+1)} &= \frac{1}{k+1} \left(4a(n, j, m, m') A_{j,m,m'}^{(k)} + 4b(n, j+1, m, m') A_{j+1,m,m'}^{(k)} \right. \\ &\quad \left. + 4c(n, j-1, m, m') A_{j-1,m,m'}^{(k)} - (n-k+1) \sum_{j=j_{\min}}^{n/2} A_{j,m,m'}^{(k-1)} \right), \end{aligned} \quad (A5)$$

with the following conditions:

$$\begin{aligned} \forall m, m', \quad A_{n/2, m, m'}^{(0)} &= 1, A_{j \neq n/2, m, m'}^{(0)} = 0, \\ \forall j, m, m', \quad A_{j, m, m'}^{(-1)} &= 0. \end{aligned} \quad (A6)$$

The first two equations are determined by the initial condition of the density matrix: $\rho(t=0) = |\phi_{\text{GHZ}}\rangle\langle\phi_{\text{GHZ}}|$. The coefficients $a(n, j, m, m')$, $b(n, j, m, m')$, and $c(n, j, m, m')$ are defined as

$$\begin{aligned} a(n, j, m, m') &= mm' \frac{1}{2j} \left(1 + \frac{(2j+1)\alpha_n^{j+1}}{(j+1)d_n^j} \right), \\ b(n, j, m, m') &= \sqrt{(j+m)(j-m)}\sqrt{(j+m')(j-m')} \frac{\alpha_n^j}{2jd_n^j}, \\ c(n, j, m, m') &= \sqrt{(j+m+1)(j-m+1)}\sqrt{(j+m'+1)(j-m'+1)} \frac{\alpha_n^{j+1}}{2(j+1)d_n^j}, \\ \alpha_n^j &= \sum_{j'=j}^{n/2} d_n^{j'}. \end{aligned}$$

To check recurrence relations, Eq. (A5), we first use the following equality [77,78]:

$$\begin{aligned} \sum_{l=1}^n \sigma_{z'}^{(l)} \overline{|j, m\rangle_{z'} \langle j, m'|} \sigma_{z'}^{(l)} &= 4 \left(a(n, j, m, m') \overline{|j, m\rangle_{z'} \langle j, m'|} + b(n, j, m, m') \overline{|j-1, m\rangle_{z'} \langle j-1, m'|} \right. \\ &\quad \left. + c(n, j, m, m') \overline{|j+1, m\rangle_{z'} \langle j+1, m'|} \right). \end{aligned} \quad (\text{A7})$$

We evaluate the application of the following action to Eq. (A3):

$$\sum_{l=1}^n \sigma_{z'}^{(l)} \left(\sum_{1 \leq l_1 < l_2 < \dots < l_k \leq n} \sigma_{z'}^{(l_1)} \sigma_{z'}^{(l_2)} \dots \sigma_{z'}^{(l_k)} \overline{|n/2, m\rangle_{z'} \langle n/2, m'|} \sigma_{z'}^{(l_1)} \sigma_{z'}^{(l_2)} \dots \sigma_{z'}^{(l_k)} \right) \sigma_{z'}^{(l)}. \quad (\text{A8})$$

By using $A_{j, m, m'}^k$, this expression can be written as

$$\begin{aligned} &\sum_{l=1}^n \sigma_{z'}^{(l)} \left(\sum_{1 \leq l_1 < l_2 < \dots < l_k \leq n} \sigma_{z'}^{(l_1)} \sigma_{z'}^{(l_2)} \dots \sigma_{z'}^{(l_k)} \overline{|n/2, m\rangle_{z'} \langle n/2, m'|} \sigma_{z'}^{(l_1)} \sigma_{z'}^{(l_2)} \dots \sigma_{z'}^{(l_k)} \right) \sigma_{z'}^{(l)} \\ &= \sum_{l=1}^n \sigma_{z'}^{(l)} \left(\sum_{j=j_{\min}}^{n/2} A_{j, m, m'}^{(k)} \overline{|j, m\rangle_{z'} \langle j, m'|} \right) \sigma_{z'}^{(l)} \\ &= 4 \sum_{j=j_{\min}}^{n/2} \left[a(n, j, m, m') A_{j, m, m'}^{(k)} + b(n, j+1, m, m') A_{j+1, m, m'}^{(k)} + c(n, j-1, m, m') A_{j-1, m, m'}^{(k)} \right] \overline{|j, m\rangle_{z'} \langle j, m'|}, \end{aligned} \quad (\text{A9})$$

where we use Eq. (A7) and the conditions $b(n, n/2+1, m, m') = b(n, j_{\min}, m, m') = 0$ and $c(n, n/2, m, m') = c(n, j_{\min}-1, m, m') = 0$ to align the summation range. In addition, note that

$$\begin{aligned} &\sum_{l=1}^n \sigma_{z'}^{(l)} \left(\sum_{1 \leq l_1 < l_2 < \dots < l_k \leq n} \sigma_{z'}^{(l_1)} \sigma_{z'}^{(l_2)} \dots \sigma_{z'}^{(l_k)} \overline{|n/2, m\rangle_{z'} \langle n/2, m'|} \sigma_{z'}^{(l_1)} \sigma_{z'}^{(l_2)} \dots \sigma_{z'}^{(l_k)} \right) \sigma_{z'}^{(l)} \\ &= (k+1) \sum_{1 \leq l_1 < l_2 < \dots < l_{k+1} \leq n} \sigma_{z'}^{(l_1)} \sigma_{z'}^{(l_2)} \dots \sigma_{z'}^{(l_{k+1})} \overline{|n/2, m\rangle_{z'} \langle n/2, m'|} \sigma_{z'}^{(l_1)} \sigma_{z'}^{(l_2)} \dots \sigma_{z'}^{(l_{k+1})} \\ &\quad + (n-k+1) \sum_{1 \leq l_1 < l_2 < \dots < l_{k-1} \leq n} \sigma_{z'}^{(l_1)} \sigma_{z'}^{(l_2)} \dots \sigma_{z'}^{(l_{k-1})} \overline{|n/2, m\rangle_{z'} \langle n/2, m'|} \sigma_{z'}^{(l_1)} \sigma_{z'}^{(l_2)} \dots \sigma_{z'}^{(l_{k-1})} \\ &= (k+1) \sum_{j=j_{\min}}^{n/2} A_{j, m, m'}^{(k+1)} \overline{|j, m\rangle_{z'} \langle j, m'|} + (n-k+1) \sum_{j=j_{\min}}^{n/2} A_{j, m, m'}^{(k-1)} \overline{|j, m\rangle_{z'} \langle j, m'|}, \end{aligned} \quad (\text{A10})$$

by a simple combinatorial calculation. By comparing the coefficients of each basis $|j, m\rangle_{z'} \langle j, m'|$ in the above two equations, we obtain the recurrence relation of Eq. (A5). Thus, we obtain the exact solution, Eq. (A4), of the dynamics with global magnetic field, collective and independent noise.

APPENDIX B: BRIEF REVIEW OF CLASSICAL AND QUANTUM FISHER INFORMATION

Here we briefly review the classical and quantum Fisher information [4]. We focus only on single parameter estimation. We assign θ to the parameter according to the main text. We note that, however, θ is not necessarily the relative angle, but a general parameter in this section. We have a density matrix ρ_θ in which the information on θ is imprinted and perform a POVM $\{\Pi_l\}$ ($\Pi_l \geq 0$, $\sum_l \Pi_l = \mathbb{I}$) on ρ_θ . From this measurement, we obtain a measurement outcome l with a probability

$$P(l|\theta) = \text{Tr}(\Pi_l \rho_\theta). \quad (\text{B1})$$

We prepare the state ρ_θ and perform POVM measurements with Π_l . Suppose that we repeat these steps M times. Now we introduce an estimator $\tilde{\theta}(\vec{l})$, which is a function of M outcomes defined as $\vec{l} = \{l_1, l_2, l_3, \dots, l_M\}$, and identify the value of this estimator as the true value of the parameter θ . The precision of the estimation is determined by the uncertainty, $\delta\theta := \sqrt{\langle (\tilde{\theta} - \theta)^2 \rangle}$, where the average ($\langle \bullet \rangle$) is defined as

$$\langle f \rangle = \sum_{\vec{l}} f(\vec{l}) \prod_{k=1}^M P(l_k|\theta), \quad (\text{B2})$$

for a function of \vec{l} . The following classical Cramér-Rao bound is satisfied for any estimator under the unbiased

condition $\langle \tilde{\theta} \rangle = \theta$,

$$\delta\theta \geq 1/\sqrt{MF_\theta(\{\Pi_l\})}, \quad (\text{B3})$$

where $F_\theta(\{\Pi_l\})$ is the Fisher information, which is defined as

$$F_\theta(\{\Pi_l\}) = \sum_l P(l|\theta) \left(\frac{\partial \log P(l|\theta)}{\partial \theta} \right)^2. \quad (\text{B4})$$

In particular, a two-valued measurement $\{\Pi, \mathbb{I} - \Pi\}$ gives

$$F_\theta(\{\Pi, \mathbb{I} - \Pi\}) = \frac{|dP(\theta)/d\theta|^2}{P(\theta)[1 - P(\theta)]}, \quad (\text{B5})$$

where $P(\theta) = \text{Tr}(\Pi \rho_\theta)$.

In quantum estimation, we can minimize the uncertainty $\delta\theta$ by choosing the best POVMs. We have the following quantum Cramér-Rao bound for any POVM $\{\Pi_l\}$:

$$F_\theta(\{\Pi_l\}) \leq F_\theta^{(Q)}, \quad (\text{B6})$$

where $F_\theta^{(Q)}$ is called the quantum Fisher information and is defined as follows:

$$F_\theta^{(Q)} = \text{Tr}(L_\theta^2 \rho_\theta), \quad \frac{\partial \rho_\theta}{\partial \theta} = \frac{1}{2} \{L_\theta, \rho_\theta\}. \quad (\text{B7})$$

By combining Eqs. (B3) and (B6), we obtain a sequence of inequalities:

$$\delta\theta \geq 1/\sqrt{MF_\theta(\{\Pi_l\})} \geq 1/\sqrt{MF_\theta^{(Q)}}. \quad (\text{B8})$$

For single-parameter estimation, it is shown that the second inequality can be saturated by taking an appropriate POVM, although that POVM may depend on the value of the parameter to be estimated.

APPENDIX C: ASYMPTOTIC SCALING BEHAVIOR

According to Eq. (A4), the survival probability $P(t)$ is given as

$$\begin{aligned} P(t) &= \langle \phi_{\text{GHZ}} | \rho(t) | \phi_{\text{GHZ}} \rangle \\ &= \sum_{k=0}^n \left(\alpha^{n-k}(t) \beta^k(t) \sum_{j=\min}^{n/2} \sum_{-j \leq m, m' \leq j} e^{-2i\Omega(m-m')t - 2\gamma_C t(m-m')^2} \rho_{m, m'} A_{j, m, m'}^{(k)} \langle \phi_{\text{GHZ}} | \overline{|j, m\rangle_{z'} \langle j, m'|} | \phi_{\text{GHZ}} \rangle \right) \\ &= \sum_{k=0}^n \left(\alpha^{n-k}(t) \beta^k(t) \sum_{-n/2 \leq m, m' \leq n/2} e^{-i2\Omega(m-m')t - 2\gamma_C t(m-m')^2} \rho_{m, m'} A_{n/2, m, m'}^{(k)} \langle \phi_{\text{GHZ}} | \overline{|n/2, m\rangle_{z'} \langle n/2, m'|} | \phi_{\text{GHZ}} \rangle \right) \\ &= \sum_{k=0}^n \left(\alpha^{n-k}(t) \beta^k(t) \sum_{-n/2 \leq m, m' \leq n/2} e^{-2i\Omega(m-m')t - 2\gamma_C t(m-m')^2} \rho_{m, m'} A_{n/2, m, m'}^{(k)} \langle \phi_{\text{GHZ}} | n/2, m, 1 \rangle_{z'} \langle n/2, m', 1 | \phi_{\text{GHZ}} \rangle \right) \\ &= \sum_{-n/2 \leq m, m' \leq n/2} \left(e^{-2i\Omega(m-m')t - 2\gamma_C t(m-m')^2} \sum_{k=0}^n \alpha^{n-k}(t) \beta^k(t) A_{n/2, m, m'}^{(k)} B_m B_{m'} \right), \end{aligned} \quad (\text{C1})$$

where we define $B_m = |\langle \phi_{\text{GHZ}} | n/2, m, 1 \rangle_{z'}|^2$. We use the fact that $\langle \text{GHZ} | j, m, i \rangle_{z'} = 0$ when $j \neq n/2$ from the first to the second line. [See also Eq. (10).] The explicit form of B_m is given as

$$\begin{aligned} B_m &= \frac{n C_{(n/2)+m}}{2^{n+1}} \left((\sqrt{1+\cos\theta})^{(n/2)+m} (-\sqrt{1-\cos\theta})^{(n/2)-m} + e^{-i\phi} (\sqrt{1-\cos\theta})^{(n/2)+m} (\sqrt{1+\cos\theta})^{(n/2)-m} \right) \\ &\quad \times \left((\sqrt{1+\cos\theta})^{(n/2)+m} (-\sqrt{1-\cos\theta})^{(n/2)-m} + e^{i\phi} (\sqrt{1-\cos\theta})^{(n/2)+m} (\sqrt{1+\cos\theta})^{(n/2)-m} \right) \\ &= \frac{n C_{(n/2)+m}}{2^{n+1}} \left((1+\cos\theta)^{(n/2)+m} (1-\cos\theta)^{(n/2)-m} + (1-\cos\theta)^{(n/2)+m} (1+\cos\theta)^{(n/2)-m} \right. \\ &\quad \left. + (e^{i\phi} + e^{-i\phi}) \sin^n \theta (-1)^{(n/2)-m} \right), \end{aligned} \quad (\text{C2})$$

where we use $\sqrt{1-\cos^2\theta} = \sin\theta$ for $0 \leq \theta \leq \pi$. Assuming $n\Omega t$, $n^2\gamma_C t$, $n\gamma_I t \ll 1$, we take the short-time perturbation in Eq. (C1) up to the first order of t :

$$\begin{aligned} P(t) &\sim \sum_{-n/2 \leq m, m' \leq n/2} \left[1 - 2i\Omega t(m-m') - 2\gamma_C t(m-m')^2 - \gamma_I t(nA_{n/2, m, m'}^{(0)} + A_{n/2, m, m'}^{(1)}) \right] B_m B_{m'} \\ &= \sum_{-n/2 \leq m, m' \leq n/2} \left[1 - 2i\Omega(m-m')t - 2\gamma_C t(m-m')^2 - \gamma_I t \left(n + \frac{4mm'}{n} \right) \right] B_m B_{m'} \\ &= \sum_{|m| \leq n/2} B_m \times \sum_{|m'| \leq n/2} B_{m'} - 2i\Omega t \left(\sum_{|m| \leq n/2} m B_m \times \sum_{|m'| \leq n/2} B_{m'} - \sum_{|m| \leq n/2} B_m \times \sum_{|m'| \leq n/2} m' B_{m'} \right) \\ &\quad - 2\gamma_C t \left(\sum_{|m| \leq n/2} m^2 B_m \times \sum_{|m'| \leq n/2} B_{m'} - 2 \sum_{|m| \leq n/2} m B_m \times \sum_{|m'| \leq n/2} m' B_{m'} + \sum_{|m| \leq n/2} B_m \times \sum_{|m'| \leq n/2} m'^2 B_{m'} \right) \\ &\quad - \gamma_I t \left(n \sum_{|m| \leq n/2} B_m \times \sum_{|m'| \leq n/2} B_{m'} + \frac{4}{n} \sum_{|m| \leq n/2} m B_m \times \sum_{|m'| \leq n/2} m' B_{m'} \right) \\ &= \left(\sum_{|m| \leq n/2} B_m \right)^2 - 4\gamma_C t \left[\sum_{|m| \leq n/2} m^2 B_m \times \sum_{|m'| \leq n/2} B_{m'} - \left(\sum_{|m| \leq n/2} m B_m \right)^2 \right] - \gamma_I t \left[n \left(\sum_{|m| \leq n/2} B_m \right)^2 + \frac{4}{n} \left(\sum_{|m| \leq n/2} m B_m \right)^2 \right]. \end{aligned} \quad (\text{C3})$$

To evaluate this quantity, we only have to calculate the following quantities:

$$\sum_{|m| \leq n/2} B_m, \quad \sum_{|m| \leq n/2} m B_m, \quad \sum_{|m| \leq n/2} m^2 B_m. \quad (\text{C4})$$

Note that the following formulae are satisfied:

$$\begin{aligned} \sum_{m=0}^n {}_n C_m X^m Y^{n-m} &= (X+Y)^n, \\ \sum_{m=0}^n m {}_n C_m X^m Y^{n-m} &= nX(X+Y)^{n-1}, \\ \sum_{m=0}^n m^2 {}_n C_m X^m Y^{n-m} &= nX(X+Y)^{n-1} + (n^2-n)X^2(X+Y)^{n-2}. \end{aligned} \quad (\text{C5})$$

We introduce a new integer variable, $\mu := m + n/2$, and let the sum range take integers. We evaluate $\sum_m B_m$ as follows:

$$\begin{aligned} \sum_{|m| \leq n/2} B_m &= \sum_{\mu=0}^n B_{\mu-n/2} = \sum_{\mu=0}^n \frac{n C_{\mu}}{2^{n+1}} (1 + \cos \theta)^{\mu} (1 - \cos \theta)^{n-\mu} + \sum_{\mu=0}^n \frac{n C_{\mu}}{2^{n+1}} (1 - \cos \theta)^{\mu} (1 + \cos \theta)^{n-\mu} \\ &\quad + (e^{i\phi} + e^{-i\phi}) \sin^n \theta \sum_{\mu=0}^n \frac{n C_{\mu}}{2^{n+1}} (-1)^{n-\mu} \\ &= \frac{2^n}{2^{n+1}} + \frac{2^n}{2^{n+1}} + (e^{i\phi} + e^{-i\phi}) \sin^n \theta \frac{(1-1)^n}{2^{n+1}} = 1. \end{aligned} \quad (\text{C6})$$

This equality is also understood in terms of the completeness of the basis $\{|n/2, m, 1\rangle_{z'}\}$ in the ($j = n/2$) subspace:

$$\begin{aligned} \sum_{|m| \leq n/2} B_m &= \sum_{|m| \leq n/2} |\langle \phi_{\text{GHZ}} | n/2, m, 1 \rangle_{z'}|^2 = \sum_{|m| \leq n/2} \langle \phi_{\text{GHZ}} | n/2, m, 1 \rangle_{z'} \langle n/2, m, 1 | \phi_{\text{GHZ}} \rangle \\ &= \langle \phi_{\text{GHZ}} | \left(\sum_{|m| \leq n/2} |n/2, m, 1\rangle_{z'} \langle n/2, m, 1| \right) | \phi_{\text{GHZ}} \rangle = \langle \phi_{\text{GHZ}} | \phi_{\text{GHZ}} \rangle = 1. \end{aligned} \quad (\text{C7})$$

Similarly, $\sum_m m B_m$ and $\sum_m m^2 B_m$ are given by

$$\begin{aligned} \sum_{|m| \leq n/2} m B_m &= \sum_{\mu=0}^n \left(\mu - \frac{n}{2} \right) B_{\mu-n/2} = \frac{n}{2^{n+1}} (1 + \cos \theta) 2^{n-1} + \frac{n}{2^{n+1}} (1 - \cos \theta) 2^{n-1} - \frac{n}{2} \sum_{\mu=0}^n B_{\mu-n/2} \\ &= \frac{n}{4} [(1 + \cos \theta) + (1 - \cos \theta)] - \frac{n}{2} = 0, \end{aligned} \quad (\text{C8})$$

and

$$\begin{aligned} \sum_{|m| \leq n/2} m^2 B_m &= \sum_{\mu=0}^n \left(\mu - \frac{n}{2} \right)^2 B_{\mu-n/2} = \sum_{\mu=0}^n \mu^2 B_{\mu-n/2} - n \sum_{\mu=0}^n \mu B_{\mu-n/2} + \frac{n^2}{4} \sum_{\mu=0}^n B_{\mu-n/2} \\ &= \frac{n}{4} [(1 + \cos \theta) + (1 - \cos \theta)] + \frac{n^2 - n}{8} [(1 + \cos \theta)^2 + (1 - \cos \theta)^2] - \frac{n^2}{4} \\ &= \frac{n}{2} + \frac{n^2 - n}{4} (1 + \cos^2 \theta) - \frac{n^2}{4} = \frac{n^2}{4} \cos^2 \theta + \frac{n}{4} (1 - \cos^2 \theta). \end{aligned} \quad (\text{C9})$$

These equations, as well as Eq. (C7), are calculated as follows:

$$\begin{aligned} \sum_{|m| \leq n/2} m B_m &= \sum_{|m| \leq n/2} m \langle \phi_{\text{GHZ}} | n/2, m, 1 \rangle_{z'} \langle n/2, m, 1 | \phi_{\text{GHZ}} \rangle = \langle \phi_{\text{GHZ}} | \sum_{|m| \leq n/2} \left(m |n/2, m, 1\rangle_{z'} \langle n/2, m, 1| \right) | \phi_{\text{GHZ}} \rangle \\ &= \langle \phi_{\text{GHZ}} | \sum_{|m| \leq n/2} \left(\frac{L_{z'}}{2} |n/2, m, 1\rangle_{z'} \langle n/2, m, 1| \right) | \phi_{\text{GHZ}} \rangle = \langle \text{GHZ} | \frac{L_{z'}}{2} | \phi_{\text{GHZ}} \rangle \\ &= \frac{1}{2} \langle \phi_{\text{GHZ}} | (\cos \theta L_z + \cos \phi \sin \theta L_x + i \sin \phi \sin \theta L_y) | \phi_{\text{GHZ}} \rangle \\ &= \frac{\cos \theta}{4} \left(\langle \frac{n}{2}, \frac{n}{2}, 1 | L_z | \frac{n}{2}, \frac{n}{2}, 1 \rangle + \langle \frac{n}{2}, -\frac{n}{2}, 1 | L_z | \frac{n}{2}, -\frac{n}{2}, 1 \rangle \right) = 0, \end{aligned} \quad (\text{C10})$$

and

$$\begin{aligned}
\sum_{|m| \leq n/2} m^2 B_m &= \langle \phi_{\text{GHZ}} | \sum_{|m| \leq n/2} \left(\frac{L_z^2}{4} |n/2, m, 1\rangle_{z'} \langle n/2, m, 1| \right) | \phi_{\text{GHZ}} \rangle = \frac{1}{4} \langle \phi_{\text{GHZ}} | L_z^2 | \phi_{\text{GHZ}} \rangle \\
&= \frac{1}{4} \langle \phi_{\text{GHZ}} | (\cos \theta L_z + \cos \phi \sin \theta L_x + i \sin \phi \sin \theta L_y)^2 | \phi_{\text{GHZ}} \rangle \\
&= \frac{1}{4} \langle \phi_{\text{GHZ}} | [\cos^2 \theta L_z^2 + \sin^2 \theta (L_+ L_- + L_- L_+)] | \phi_{\text{GHZ}} \rangle \\
&= \frac{n^2}{4} \cos^2 \theta + \frac{n}{4} (1 - \cos^2 \theta). \tag{C11}
\end{aligned}$$

By using the above equations, we obtain Eq. (20).

APPENDIX D: θ DEPENDENCE OF τ_c

Here we analyze the sensitivity in protocol D_{non} . If n satisfies the condition $n \ll 1/\sqrt{\gamma_0 \tau_c}$, we can take a time region where both the condition $\tau_c \ll t \ll 1/n^2 \gamma_0$ are satisfied. In this region, the survival probability $P(t) = \langle \phi_{\text{GHZ}} | \rho(t) | \phi_{\text{GHZ}} \rangle$ is given by

$$\begin{aligned}
P(t) &\sim 1 - \gamma_C(t) t [n^2 \cos^2 \theta + n(1 - \cos^2 \theta)] - \gamma_I t n \\
&\sim 1 - \gamma_0 \tau_c (-1 + e^{-t/\tau_c} + t/\tau_c) [n^2 \cos^2 \theta + n(1 - \cos^2 \theta)] - \gamma_I t n, \\
&\sim 1 - \gamma_0 t [n^2 \cos^2 \theta + n(1 - \cos^2 \theta)] - \gamma_I t n, \tag{D1}
\end{aligned}$$

where we use the short-time perturbation with the conditions $n^2 \gamma(t) t, n \gamma_I t \ll 1$ in the first line and $\gamma_C(t) \simeq \gamma_0$ in the third line. We also assume $n \gamma_I t \ll 1$ in Eq. (D1). In the time region where the survival probability is written in Eq. (D1), the same manner as in protocol D shows that the uncertainty of protocol D_{non} approaches the HL: by assigning $t = t_0/n^2$ ($\gamma_0 t_0 \ll 1$), the simple calculation gives

$$\delta\theta^{\min}(n) = \frac{\sqrt{P(t)[1-P(t)]}}{|dP(t)/d\theta| \sqrt{T n^2/t_0}} \sim \frac{\sqrt{\gamma_0 t_0 \cos^2 \theta}}{|\gamma_0 t_0 \sin(2\theta)| \sqrt{T n^2/t_0}} = \frac{1}{2n \sqrt{\gamma_0 T} \sin \theta}, \quad n \ll 1/\sqrt{\gamma_0 \tau_c}, \tag{D2}$$

where we explicitly show that $\delta\theta^{\min}$ is a function of n . Meanwhile, for large n where the condition $n \ll 1/\sqrt{\gamma_0 \tau_c}$ is not met, we cannot take t satisfying both the conditions $n^2 \gamma_0 t \ll 1$ and $\tau_c \ll t$. Although we do not know what kind of scaling is realized in this region, the numerical calculations shown in Fig. 3 suggest the SQL will be attained. Thus, we roughly model the uncertainty $\delta\theta^{\min}$ in protocol D_{non} as

$$\delta\theta^{\min}(n) = \begin{cases} \frac{1}{2n \sqrt{\gamma_0 T} \sin \theta}, & n < \alpha / \sqrt{\gamma_0 \tau_c}, \\ \frac{K}{\sqrt{n \gamma_0 T}}, & n > \alpha / \sqrt{\gamma_0 \tau_c}, \end{cases} \tag{D3}$$

where α is such a small number that the condition $n \ll 1/\sqrt{\gamma_0 \tau_c}$ holds and K is a constant, which is fixed in order that the line connects, i.e., $1/2n \sqrt{\gamma_0 T} \sin \theta = K/\sqrt{n \gamma_0 T}$, at $n = \alpha/\sqrt{\gamma_0 \tau_c}$. On the other hand, the uncertainty $\delta\theta^{(\mathcal{Q})\min}$ of protocol F is crudely given as

$$\delta\theta^{(\mathcal{Q})\min}(n) = \frac{C}{\sqrt{n \gamma_0 T}}, \tag{D4}$$

according to the numerical calculations (Fig. 3). Here C is assumed to be almost independent of θ as suggested in Fig. 3. We just put γ_0 in Eq. (D4) in order to nondimensionalize $\delta\theta^{(\mathcal{Q})\min}(n)$.

The condition for $\delta\theta^{\min}$ to overcome $\delta\theta^{(\mathcal{Q})\min}$ is given by

$$\delta\theta^{\min}(\alpha/\sqrt{\gamma_0 \tau_c}) \leq \delta\theta^{(\mathcal{Q})\min}(\alpha/\sqrt{\gamma_0 \tau_c}). \tag{D5}$$

We obtain the rough requirement for τ_c from this inequality as

$$\tau_c \leq \tau_{\text{lim}}^\theta := \frac{\alpha^2 (2C \sin \theta)^4}{\gamma_0}. \tag{D6}$$

τ_{lim}^θ characterizes whether $\delta\theta^{\min}$ overcomes $\delta\theta^{(\mathcal{Q})\min}$ in this toy model. For different parameters θ and θ' , the ratio $\tau_{\text{lim}}^{\theta'}/\tau_{\text{lim}}^\theta$ behaves as $(\sin \theta'/\sin \theta)^4$. When we assign $\theta = 1.0$ rad and $\theta' = 0.5$ rad, we obtain

$$\tau_{\text{lim}}^{\theta=0.5}/\tau_{\text{lim}}^{\theta=1.0} = [\sin(0.5)/\sin(1.0)]^4 \sim (0.569)^4 \sim 0.105. \tag{D7}$$

Thus, even though the two values $\theta = 1.0$ rad and $\theta' = 0.5$ rad have only a factor-of-2 difference, the requirement on τ_c can be tightened by an order of magnitude, as shown in Fig. 3.

-
- [1] M. E. Huber, N. C. Koshnick, H. Bluhm, L. J. Archuleta, T. Azua, P. G. Björnsson, B. W. Gardner, S. T. Halloran, E. A. Lucero, and K. A. Moler, Gradiometric micro-squid susceptometer for scanning measurements of mesoscopic samples, *Rev. Sci. Instrum.* **79**, 053704 (2008).
- [2] E. Ramsden, *Hall-Effect Sensors: Theory and Application* (Elsevier, London, 2011).
- [3] M. Poggio and C. L. Degen, Force-detected nuclear magnetic resonance: Recent advances and future challenges, *Nanotechnology* **21**, 342001 (2010).
- [4] C. W. Helstrom, *Quantum Detection and Estimation Theory* (Academic Press, New York, 1976), Vol. 84.
- [5] J. A. Dunningham, Using quantum theory to improve measurement precision, *Contemp. Phys.* **47**, 257 (2006).
- [6] A. S. Holevo, *Probabilistic and Statistical Aspects of Quantum Theory* (Springer Science & Business Media, Berlin, 2011), Vol. 1.
- [7] C. M. Caves, Quantum-mechanical noise in an interferometer, *Phys. Rev. D* **23**, 1693 (1981).
- [8] V. Giovannetti, S. Lloyd, and L. Maccone, Quantum-enhanced measurements: Beating the standard quantum limit, *Science* **306**, 1330 (2004).
- [9] V. Giovannetti, S. Lloyd, and L. Maccone, Quantum Metrology, *Phys. Rev. Lett.* **96**, 010401 (2006).
- [10] D. S. Simon, G. Jaeger, and A. V. Sergienko, in *Quantum Metrology, Imaging, and Communication* (Springer, 2017), p. 91.
- [11] V. Giovannetti, S. Lloyd, and L. Maccone, Advances in quantum metrology, *Nat. Photonics* **5**, 222 (2011).
- [12] M. A. Taylor and W. P. Bowen, Quantum metrology and its application in biology, *Phys. Rep.* **615**, 1 (2016).
- [13] C. L. Degen, F. Reinhard, and P. Cappellaro, Quantum sensing, *Rev. Mod. Phys.* **89**, 035002 (2017).
- [14] M. G. Paris, Quantum estimation for quantum technology, *Int. J. Quantum Inf.* **7**, 125 (2009).
- [15] D. J. Wineland, J. J. Bollinger, W. M. Itano, F. Moore, and D. Heinzen, Spin squeezing and reduced quantum noise in spectroscopy, *Phys. Rev. A* **46**, R6797 (1992).
- [16] D. J. Wineland, J. J. Bollinger, W. M. Itano, and D. Heinzen, Squeezed atomic states and projection noise in spectroscopy, *Phys. Rev. A* **50**, 67 (1994).
- [17] G. Tóth and I. Apellaniz, Quantum metrology from a quantum information science perspective, *J. Phys. A: Math. Theor.* **47**, 424006 (2014).
- [18] J. J. Bollinger, W. M. Itano, D. J. Wineland, and D. J. Heinzen, Optimal frequency measurements with maximally correlated states, *Phys. Rev. A* **54**, R4649 (1996).
- [19] K. Macieszczak, Zeno limit in frequency estimation with non-markovian environments, *Phys. Rev. A* **92**, 010102 (2015).
- [20] S. F. Huelga, C. Macchiavello, T. Pellizzari, A. K. Ekert, M. B. Plenio, and J. I. Cirac, Improvement of Frequency Standards with Quantum Entanglement, *Phys. Rev. Lett.* **79**, 3865 (1997).
- [21] A. Górecka, F. A. Pollock, P. Liuzzo-Scorpo, R. Nichols, G. Adesso, and K. Modi, Noisy frequency estimation with noisy probes, *New J. Phys.* **20**, 083008 (2018).
- [22] M. A. Rossi, F. Albarelli, D. Tamascelli, and M. G. Genoni, Noisy Quantum Metrology Enhanced by Continuous Non-demolition Measurement, *Phys. Rev. Lett.* **125**, 200505 (2020).
- [23] S. Altenburg, M. Oszmaniec, S. Wölk, and O. Gühne, Estimation of gradients in quantum metrology, *Phys. Rev. A* **96**, 042319 (2017).
- [24] S. Schmitt, T. Gefen, F. M. Stürner, T. Unden, G. Wolff, C. Müller, J. Scheuer, B. Naydenov, M. Markham, S. Pezzagna, *et al.*, Submillihertz magnetic spectroscopy performed with a nanoscale quantum sensor, *Science* **356**, 832 (2017).
- [25] M. Ledbetter, K. Jensen, R. Fischer, A. Jarmola, and D. Budker, Gyroscopes based on nitrogen-vacancy centers in diamond, *Phys. Rev. A* **86**, 052116 (2012).
- [26] A. Ajoy and P. Cappellaro, Stable three-axis nuclear-spin gyroscope in diamond, *Phys. Rev. A* **86**, 062104 (2012).
- [27] T. Monz, P. Schindler, J. T. Barreiro, M. Chwalla, D. Nigg, W. A. Coish, M. Harlander, W. Hänsel, M. Hennrich, and R. Blatt, 14-Qubit Entanglement: Creation and Coherence, *Phys. Rev. Lett.* **106**, 130506 (2011).
- [28] D. M. Greenberger, M. A. Horne, A. Shimony, and A. Zeilinger, Bell's theorem without inequalities, *Am. J. Phys.* **58**, 1131 (1990).
- [29] L. DiCarlo, M. D. Reed, L. Sun, B. R. Johnson, J. M. Chow, J. M. Gambetta, L. Frunzio, S. M. Girvin, M. H. Devoret, and R. J. Schoelkopf, Preparation and measurement of three-qubit entanglement in a superconducting circuit, *Nature* **467**, 574 (2010).
- [30] M. Holland and K. Burnett, Interferometric Detection of Optical Phase Shifts at the Heisenberg Limit, *Phys. Rev. Lett.* **71**, 1355 (1993).
- [31] T. Nagata, R. Okamoto, J. L. O'Brien, K. Sasaki, and S. Takeuchi, Beating the standard quantum limit with four-entangled photons, *Science* **316**, 726 (2007).
- [32] J. A. Jones, S. D. Karlen, J. Fitzsimons, A. Ardavan, S. C. Benjamin, G. A. D. Briggs, and J. J. Morton, Magnetic field sensing beyond the standard quantum limit using 10-spin noon states, *Science* **324**, 1166 (2009).
- [33] A. Facon, E.-K. Dietsche, D. Grosso, S. Haroche, J.-M. Raimond, M. Brune, and S. Gleyzes, A sensitive electrometer based on a Rydberg atom in a Schrödinger-cat state, *Nature* **535**, 262 (2016).
- [34] I. Kruse, K. Lange, J. Peise, B. Lücke, L. Pezzè, J. Arlt, W. Ertmer, C. Lisdat, L. Santos, A. Smerzi, *et al.*, Improvement of an Atomic Clock Using Squeezed Vacuum, *Phys. Rev. Lett.* **117**, 143004 (2016).
- [35] K. C. Cox, G. P. Greve, J. M. Weiner, and J. K. Thompson, Deterministic Squeezed States with Collective Measurements and Feedback, *Phys. Rev. Lett.* **116**, 093602 (2016).
- [36] O. Hosten, N. J. Engelsen, R. Krishnakumar, and M. A. Kasevich, Measurement noise 100 times lower than the quantum-projection limit using entangled atoms, *Nature* **529**, 505 (2016).

- [37] X.-Y. Luo, Y.-Q. Zou, L.-N. Wu, Q. Liu, M.-F. Han, M. K. Tey, and L. You, Deterministic entanglement generation from driving through quantum phase transitions, *Science* **355**, 620 (2017).
- [38] D. Mason, J. Chen, M. Rossi, Y. Tsaturyan, and A. Schliesser, Continuous force and displacement measurement below the standard quantum limit, *Nat. Phys.* **15**, 745 (2019).
- [39] H. Bao, J. Duan, S. Jin, X. Lu, P. Li, W. Qu, M. Wang, I. Novikova, E. E. Mikhailov, K.-F. Zhao, *et al.*, Spin squeezing of 10 11 atoms by prediction and retrodiction measurements, *Nature* **581**, 159 (2020).
- [40] E. Pedrozo-Peñafiel, S. Colombo, C. Shu, A. F. Adiyatullin, Z. Li, E. Mendez, B. Braverman, A. Kawasaki, D. Akamatsu, Y. Xiao, *et al.*, Entanglement on an optical atomic-clock transition, *Nature* **588**, 414 (2020).
- [41] A. Shaji and C. M. Caves, Qubit metrology and decoherence, *Phys. Rev. A* **76**, 032111 (2007).
- [42] Y. Matsuzaki, S. C. Benjamin, and J. Fitzsimons, Magnetic field sensing beyond the standard quantum limit under the effect of decoherence, *Phys. Rev. A* **84**, 012103 (2011).
- [43] A. W. Chin, S. F. Huelga, and M. B. Plenio, Quantum Metrology in Non-Markovian Environments, *Phys. Rev. Lett.* **109**, 233601 (2012).
- [44] R. Demkowicz-Dobrzański, J. Kołodyński, and M. Guţă, The elusive Heisenberg limit in quantum-enhanced metrology, *Nat. Commun.* **3**, 1 (2012).
- [45] R. Chaves, J. Brask, M. Markiewicz, J. Kołodyński, and A. Acín, Noisy Metrology Beyond the Standard Quantum Limit, *Phys. Rev. Lett.* **111**, 120401 (2013).
- [46] T. Tanaka, P. Knott, Y. Matsuzaki, S. Dooley, H. Yamaguchi, W. J. Munro, and S. Saito, Proposed Robust Entanglement-Based Magnetic Field Sensor Beyond the Standard Quantum Limit, *Phys. Rev. Lett.* **115**, 170801 (2015).
- [47] E. Davis, G. Bentsen, and M. Schleier-Smith, Approaching the Heisenberg Limit Without Single-Particle Detection, *Phys. Rev. Lett.* **116**, 053601 (2016).
- [48] Y. Matsuzaki, S. Benjamin, S. Nakayama, S. Saito, and W. J. Munro, Quantum Metrology Beyond the Classical Limit Under the Effect of Dephasing, *Phys. Rev. Lett.* **120**, 140501 (2018).
- [49] L. B. Ho, H. Hakoshima, Y. Matsuzaki, M. Matsuzaki, and Y. Kondo, Multiparameter quantum estimation under dephasing noise, *Phys. Rev. A* **102**, 022602 (2020).
- [50] A. Yoshinaga, M. Tatsuta, and Y. Matsuzaki, Entanglement-enhanced sensing using a chain of qubits with always-on nearest-neighbor interactions, *Phys. Rev. A* **103**, 062602 (2021).
- [51] E. M. Kessler, I. Lovchinsky, A. O. Sushkov, and M. D. Lukin, Quantum Error Correction for Metrology, *Phys. Rev. Lett.* **112**, 150802 (2014).
- [52] G. Arrad, Y. Vinkler, D. Aharonov, and A. Retzker, Increasing Sensing Resolution with Error Correction, *Phys. Rev. Lett.* **112**, 150801 (2014).
- [53] W. Dür, M. Skotiniotis, F. Froewis, and B. Kraus, Improved Quantum Metrology Using Quantum Error Correction, *Phys. Rev. Lett.* **112**, 080801 (2014).
- [54] D. A. Herrera-Martí, T. Gefen, D. Aharonov, N. Katz, and A. Retzker, Quantum Error-Correction-Enhanced Magnetometer Overcoming the Limit Imposed by Relaxation, *Phys. Rev. Lett.* **115**, 200501 (2015).
- [55] Y. Matsuzaki and S. Benjamin, Magnetic-field sensing with quantum error detection under the effect of energy relaxation, *Phys. Rev. A* **95**, 032303 (2017).
- [56] T. Unden, P. Balasubramanian, D. Louzon, Y. Vinkler, M. B. Plenio, M. Markham, D. Twitchen, A. Stacey, I. Lovchinsky, A. O. Sushkov, *et al.*, Quantum Metrology Enhanced by Repetitive Quantum Error Correction, *Phys. Rev. Lett.* **116**, 230502 (2016).
- [57] L. Cohen, Y. Pilnyak, D. Istrati, A. Retzker, and H. Eisenberg, Demonstration of a quantum error correction for enhanced sensitivity of photonic measurements, *Phys. Rev. A* **94**, 012324 (2016).
- [58] Y. Matsuzaki, T. Shimo-Oka, H. Tanaka, Y. Tokura, K. Semba, and N. Mizuochi, Hybrid quantum magnetic-field sensor with an electron spin and a nuclear spin in diamond, *Phys. Rev. A* **94**, 052330 (2016).
- [59] D. Averin, K. Xu, Y.-P. Zhong, C. Song, H. Wang, and S. Han, Suppression of Dephasing by Qubit Motion in Superconducting Circuits, *Phys. Rev. Lett.* **116**, 010501 (2016).
- [60] M. Beau and A. del Campo, Nonlinear Quantum Metrology of Many-Body Open Systems, *Phys. Rev. Lett.* **119**, 010403 (2017).
- [61] Y. Matsuzaki, S. Saito, and W. J. Munro, Quantum metrology at the Heisenberg limit with the presence of independent dephasing, *ArXiv:1809.00176* (2018).
- [62] D. Braun and J. Martin, Heisenberg-limited sensitivity with decoherence-enhanced measurements, *Nat. Commun.* **2**, 1 (2011).
- [63] R. Demkowicz-Dobrzański, J. Czajkowski, and P. Sekatski, Adaptive Quantum Metrology Under General Markovian Noise, *Phys. Rev. X* **7**, 041009 (2017).
- [64] P. Sekatski, M. Skotiniotis, J. Kołodyński, and W. Dür, Quantum metrology with full and fast quantum control, *Quantum* **1**, 27 (2017).
- [65] S. Dooley, M. Hanks, S. Nakayama, W. J. Munro, and K. Nemoto, Robust quantum sensing with strongly interacting probe systems, *npj Quantum Inf.* **4**, 1 (2018).
- [66] B. Koczor, S. Endo, T. Jones, Y. Matsuzaki, and S. C. Benjamin, Variational-state quantum metrology, *New J. Phys.* **22**, 083038 (2020).
- [67] P. Komar, E. M. Kessler, M. Bishof, L. Jiang, A. S. Sørensen, J. Ye, and M. D. Lukin, A quantum network of clocks, *Nat. Phys.* **10**, 582 (2014).
- [68] Z. Eldredge, M. Foss-Feig, J. A. Gross, S. L. Rolston, and A. V. Gorshkov, Optimal and secure measurement protocols for quantum sensor networks, *Phys. Rev. A* **97**, 042337 (2018).
- [69] K. Qian, Z. Eldredge, W. Ge, G. Pagano, C. Monroe, J. V. Porto, and A. V. Gorshkov, Heisenberg-scaling measurement protocol for analytic functions with quantum sensor networks, *Phys. Rev. A* **100**, 042304 (2019).
- [70] T. J. Proctor, P. A. Knott, and J. A. Dunningham, Multiparameter Estimation in Networked Quantum Sensors, *Phys. Rev. Lett.* **120**, 080501 (2018).
- [71] Y. Takeuchi, Y. Matsuzaki, K. Miyanishi, T. Sugiyama, and W. J. Munro, Quantum remote sensing with asymmetric information gain, *Phys. Rev. A* **99**, 022325 (2019).

- [72] X. Guo, C. R. Breum, J. Borregaard, S. Izumi, M. V. Larsen, T. Gehring, M. Christandl, J. S. Neergaard-Nielsen, and U. L. Andersen, Distributed quantum sensing in a continuous-variable entangled network, *Nat. Phys.* **16**, 281 (2020).
- [73] H. Kasai, Y. Takeuchi, H. Hakoshima, Y. Matsuzaki, and Y. Tokura, Anonymous quantum sensing, *ArXiv:2105.05585* (2021).
- [74] H.-P. Breuer, E.-M. Laine, J. Piilo, and B. Vacchini, Colloquium: Non-Markovian dynamics in open quantum systems, *Rev. Mod. Phys.* **88**, 021002 (2016).
- [75] V. Mihailov, Addition or arbitrary number of identical angular momenta, *J. Phys. A: Math. Gen.* **10**, 147 (1977).
- [76] J. Ping, F. Wang, and J.-Q. Chen, *Group Representation Theory for Physicists* (World Scientific Publishing Company, Singapore, 2002).
- [77] B. A. Chase and J. Geremia, Collective processes of an ensemble of spin-1/2 particles, *Phys. Rev. A* **78**, 052101 (2008).
- [78] B. Q. Baragiola, B. A. Chase, and J. Geremia, Collective uncertainty in partially polarized and partially decohered spin-1/2 systems, *Phys. Rev. A* **81**, 032104 (2010).
- [79] I. Urizar-Lanz, P. Hyllus, I. L. Egusquiza, M. W. Mitchell, and G. Tóth, Macroscopic singlet states for gradient magnetometry, *Phys. Rev. A* **88**, 013626 (2013).
- [80] P. Sekatski, S. Wölk, and W. Dür, Optimal distributed sensing in noisy environments, *Phys. Rev. Res.* **2**, 023052 (2020).
- [81] A. Einstein, Zur elektrodynamik bewegter körper, *Ann. Phys.* **322**, 891 (1905).
- [82] R. Jozsa, D. S. Abrams, J. P. Dowling, and C. P. Williams, Quantum Clock Synchronization Based on Shared Prior Entanglement, *Phys. Rev. Lett.* **85**, 2010 (2000).
- [83] E. O. Ilo-Okeke, L. Tessler, J. P. Dowling, and T. Byrnes, Remote quantum clock synchronization without synchronized clocks, *npj Quantum Inf.* **4**, 1 (2018).
- [84] W. Gerlach and O. Stern, Der experimentelle nachweis des magnetischen moments des silberatoms, *Z. Phys.* **8**, 110 (1922).
- [85] M. H. Levitt, *Spin Dynamics: Basics of Nuclear Magnetic Resonance* (Wiley, New York, NY, 2001), <https://cds.cern.ch/record/500323>.
- [86] E. Togan, Y. Chu, A. S. Trifonov, L. Jiang, J. Maze, L. Childress, M. G. Dutt, A. S. Sørensen, P. R. Hemmer, A. S. Zibrov, *et al.*, Quantum entanglement between an optical photon and a solid-state spin qubit, *Nature* **466**, 730 (2010).
- [87] L.-m. Liang, *et al.*, Realization of quantum swap gate between flying and stationary qubits, *Phys. Rev. A* **72**, 024303 (2005).
- [88] S. Yang, Y. Wang, D. B. Rao, T. H. Tran, A. S. Momenzadeh, M. Markham, D. Twitchen, P. Wang, W. Yang, R. Stöhr, *et al.*, High-fidelity transfer and storage of photon states in a single nuclear spin, *Nat. Photonics* **10**, 507 (2016).
- [89] H. Kosaka and N. Niikura, Entangled Absorption of a Single Photon with a Single Spin in Diamond, *Phys. Rev. Lett.* **114**, 053603 (2015).
- [90] B. Scharfenberger, H. Kosaka, W. J. Munro, and K. Nemoto, Absorption-based quantum communication with NV centres, *New J. Phys.* **17**, 103012 (2015).
- [91] N. Samkharadze, G. Zheng, N. Kalhor, D. Brousse, A. Sammak, U. Mendes, A. Blais, G. Scappucci, and L. Vandersypen, Strong spin-photon coupling in silicon, *Science* **359**, 1123 (2018).
- [92] N. Nishizawa, K. Nishibayashi, and H. Munekata, Pure circular polarization electroluminescence at room temperature with spin-polarized light-emitting diodes, *Proc. Natl. Acad. Sci.* **114**, 1783 (2017).
- [93] K. Miyamoto, H. Wortelen, T. Okuda, J. Henk, and M. Donath, Circular-polarized-light-induced spin polarization characterized for the dirac-cone surface state at $w(110)$ with c_{2v} symmetry, *Sci. Rep.* **8**, 1 (2018).
- [94] Y. Kondo, M. Nakahara, S. Tanimura, S. Kitajima, C. Uchiyama, and F. Shibata, Generation and suppression of decoherence in artificial environment for qubit system, *J. Phys. Soc. Jpn.* **76**, 074002 (2007).
- [95] T. Kohmoto, Y. Fukuda, M. Kunitomo, K. Ishikawa, Y. Takahashi, K. Ebina, and M. Kaburagi, Hole burning in a well-characterized noise field: Nonadherence to the Bloch equations, *Phys. Rev. B* **52**, 13475 (1995).
- [96] G. Teklemariam, E. Fortunato, C. López, J. Emerson, J. P. Paz, T. Havel, and D. Cory, Method for modeling decoherence on a quantum-information processor, *Phys. Rev. A* **67**, 062316 (2003).